



Contents lists available at ScienceDirect

Journal of the European Ceramic Society

journal homepage: www.elsevier.com/locate/jeurceramsoc

Original Article

Grain boundary corrosion in TiO₂ bone scaffolds doped with group II cationsAnne Klemm^a, Manuel Gomez-Florit^{b,c}, Patricia Almeida Carvalho^d, Mattis Wachendörfer^{a,e},
Manuela E. Gomes^{b,c}, Håvard J. Haugen^a, Hanna Tiainen^{a,*}^a University of Oslo, Department of Biomaterials, Institute of Clinical Dentistry, P.O. Box 1109 Blindern, 0317, Oslo, Norway^b 3B's Research Group, I3Bs – Research Institute on Biomaterials, Biodegradables and Biomimetics, University of Minho, Headquarters of the European Institute of Excellence on Tissue Engineering and Regenerative Medicine, AvePark, Parque de Ciência e Tecnologia, Zona Industrial da Gandra, 4805-017, Barco, Guimarães, Portugal^c ICVS/3B's-PT Government Associate Laboratory, Braga, Guimarães, Portugal^d SINTEF Materials and Chemistry, PB 124, Blindern, NO-0314, Oslo, Norway^e Helmholtz-Institute for Biomedical Engineering, Chair of Medical Engineering, RWTH Aachen University, Pauwelsstraße 20, 52074, Aachen, Germany

ARTICLE INFO

Keywords:

Doped TiO₂

Corrosion

Grain boundary

SrTiO₃

Osteogenic differentiation

ABSTRACT

A pH drop during the inflammatory phase during bone regeneration can cause corrosion in TiO₂ bone scaffolds and the loss of compressive strength. Corrosion as ion leaching and dissolution is confined to grain boundaries. Cationic doping of TiO₂ showed to increase the compressive strength but increased the amount of impurities in grain boundaries as well. Therefore, this study showed the different grain boundary formation for Ca, Sr and Mg doped scaffolds and their corrosion behavior. After corrosion, the amorphous phase in grain boundaries was dissolved in all doped scaffolds. Differences occurred due to the formation of an additional crystalline phase in Sr doped scaffolds. The presence of an amorphous and crystalline phase led to an inhomogeneous dissolution in grain boundaries and a significant decrease in compressive strength already after 4 h in contact with an acidic environment. Released ions did not show any cytotoxic effect on hASCs. Mg doped TiO₂ scaffolds led to significant increased osteogenic differentiation.

1. Introduction

The potential for highly porous TiO₂ scaffolds as bone scaffolds is well-known [1–3]. Due to a sufficient pore size, interconnectivity and large surface-to-volume ratio, these scaffolds allow cell ingrowth, vascularization and cell adhesion [2,3]. Furthermore, TiO₂ scaffolds produced by the polymer sponge replication method combine high porosity with high compressive strength [4]. This property of bone scaffolds is crucial for the support of bone cells during bone regeneration process and should be stable during the inflammatory phase.

To reach a compressive strength similar to that of natural bone (2–12 MPa), different strategies have been proposed to increase the strength of TiO₂ scaffolds. One possible strategy is the so-called double coating, where the final sintered scaffolds are coated with a low viscous slurry to densify the strut architecture. Using this strategy, the compressive strength of TiO₂ scaffolds can be increased from approx. 1 MPa up to 1.6 MPa for a porosity of approx. 90% [4]. We have also shown that cationic doping of TiO₂ slurries leads to a similar significant increase in compressive strength. The advantage of this strategy is that no additional step, including low viscous slurry and sintering procedure, is necessary. By adding different ions to the slurry, two mechanisms lead

to higher compressive strength. First, the slurry viscosity is increased, which was shown to affect the final strength. Second, the sintering behavior of TiO₂ is changed and the presence of a liquid phase during sintering was proposed as reason for the improved strut densification and a high compressive strength of 1.64 MPa [5].

Corrosion resistance of the TiO₂ scaffolds is an important property to ensure a high compressive strength during inflammatory phase. During inflammatory phase, a large amount of macrophages are present which can acidify their microenvironment to a pH level of 3.6–3.7 [6]. Ceramics in general show corrosion in acidic environments due to ion leaching and dissolution [7]. These effects tend to concentrate on areas where crystal lattice defects are dominant, such as grain boundaries. Müller et al. found released Si and Al from TiO₂ grain boundaries after storing the TiO₂ bone scaffolds for 8 weeks in 1 mM HCl solution (pH3). Furthermore, the study showed significant decrease in compressive strength after corrosion [8].

In the present study, TiO₂ scaffolds doped with divalent Ca, Sr and Mg cations showed a different and new impurity rich formation in grain boundaries. Considering that corrosion is likely to occur in these areas, the new formation has to be investigated with focus on corrosion behavior. TEM was used to investigate the grain boundary formation in

* Corresponding author.

E-mail address: Hanna.tiainen@odont.uio.no (H. Tiainen).<https://doi.org/10.1016/j.jeurceramsoc.2018.12.055>

Received 24 October 2018; Received in revised form 16 December 2018; Accepted 22 December 2018

0955-2219/© 2018 Elsevier Ltd. All rights reserved.

Ca, Sr and Mg doped TiO₂ scaffolds. Additionally, a short corrosion test showed the corrosion resistance and amorphous or crystalline nature of phases in grain boundaries. Biocompatibility of these doped scaffolds was investigated by LDH, real-time PCR and live-dead staining which showed the effect of released ions on cell differentiation.

2. Material and methods

2.1. Scaffold fabrication

The polymer foam replication method was used to fabricate TiO₂ scaffolds as previously described [5]. The slurry was prepared by adding 65 g of anatase powder (HOMBITAN FF-Pharma, Sachtleben Chemie GmbH, Duisburg, Germany) into 25 ml of divalent salt solutions. For investigating the scaffold properties depending on salt concentration, the scaffolds were fabricated with increasing salt concentrations up to 0.1 M in 0.02 M steps using the divalent salts CaCl₂, MgCl₂ and SrCl₂ dissolved in deionised water (dH₂O). The slurry was adjusted to a work pH 1.5–1.7 by adding 1 M HCl and was stirred at 5000 rpm for 2.5 h at a temperature of 15–17 °C (Dispermat Ca-40, VMA-Gertsmann GmbH, Reichshof, Germany).

After coating the polymer foams (60 pores per inch, diameter 10 mm, height 10 mm, Bulbern S, Eurofoam GmbH, Wiesbaden, Germany) with the different slurries, excess slurry was squeezed out and the samples dried for 24 h at room temperature. Burn out of the polymer was performed at 1100 °C for 5 h (heating rate of 1 K/min) and sintering at 1500 °C for 20 h (heating rate 3 K/min) (HTC-08/16, Nabertherm GmbH, Lilienthal, Germany).

2.2. Corrosion test

Long-term corrosion test was performed for the control group without salt and 0.1 M CaCl₂, MgCl₂ and SrCl₂ scaffolds. The scaffolds were stored in polypropylene tubes for 2, 4 and 8 weeks in dH₂O and 1 mM HCl (pH3) solution at 37 °C. The short-term test was performed for scaffolds fabricated with different salt concentrations in 1 mM HCl solution at 37 °C for 4 h, 24 h and 7 d. After storing scaffolds in HCl solution, the scaffolds were rinsed with dH₂O and dried for 24 h at 37 °C.

2.3. Atomic absorption spectroscopy (AAS)

To measure the amount of released ions due to corrosion, samples were prepared in the same way as for the corrosion test. After 4 h, 1 d, 3 d and 7 d, the acidic solutions were filtered using a 0.2 µm PES filter. Ca and Mg samples were mixed with LaCl₃ (100:1). The amount of Ca, Mg and Sr was measured using an atomic absorption spectroscope (Perkin Elmer AANALYST 400, PerkinElmer, Massachusetts, USA). Three independent samples were measured two times and the average ± standard deviation is shown.

2.4. Compressive strength

Compressive strength of all fabricated scaffolds (uncorroded and corroded) were measured by using an uniaxial mechanical testing machine (Zwick/Roell Z2.5; Zwick GmbH & Co. KG, Ulm, Germany). After reaching the preload of 0.5 N, the scaffolds were compressed along their long axis (1 kN load cell) with a testing speed of 100 mm/min until failure, which is defined as 15% of the highest measured peak. The compressive strength on the basis of scaffold diameter and maximum force until failure was calculated with the software Test Expert II.

2.5. Scanning electron microscopy (SEM) and energy dispersive X-ray spectroscopy (EDX)

For the visual control of grain boundary corrosion, SEM (TM3030,

Hitachi High-Technologies Europe GmbH, Krefeld, Germany) and EDX (Quantax 70, Bruker, Billerica, USA) were used. Scaffolds (n = 3) were mounted on aluminium stubs with conductive carbon tape. Images were taken with backscattered electrons mode and at 15 kV accelerating voltage. Scaffolds used for cell studies were washed with PBS and cells were fixed with 2.5% glutaraldehyde and stored for 1 h at 4 °C. After washing again with PBS, cells were dehydrated with increasing ethanol solutions (50, 70, 90 and 100%). After immersing samples three times with HDMS and drying overnight, the SEM (JSM-6010 LV, JEOL, Japan) was operated at 15 kV.

2.6. Focused ion beam (FIB) and transmission electron microscopy (TEM)

TEM samples were prepared by FIB using a JIB-4500 MultiBeam SEM-FIB (JOEL, USA). Scaffolds were embedded in epoxy resin (Poxy Pak™ Epoxy, Ted Pella, Inc., Sweden) mixed with 50 wt% carbon powder (PELCO® Carbon (Graphite) Powder, Ted Pella, Inc., Sweden) to mitigate charging effects. Samples were grinded and then coated with 7 nm thick platinum coating. The grain boundary formation was investigated using a Titan G2 60–300 microscope (FEI Company, USA). Three different selected area diffraction (SAD) patterns were recorded and the crystal structure was determined using JEMS (JEMS-SAAS, Switzerland) and VESTA (JP-Minerals, Japan).

2.7. Human adipose stem cells (hASC) culture

hASCs were isolated from lipoaspirate samples. Samples were obtained from the abdominal region of the patients undergoing plastic surgery, under the scope of previously established protocols with Hospital da Prelada (Porto, Portugal) with the approval of the University of Minho Ethics Committee.

Scaffolds were placed in non-adherent 48 well plates. 3×10^5 cells (hASCs) in 800 µl αMEM media were added against the well wall to each sample. After 3 h shaking the scaffolds at 37 °C, the scaffolds were moved to new well plates and 500 µl fresh αMEM media without cells was added. The used αMEM was supplemented with sodium bicarbonate, 10% fetal bovine serum and 1% antibiotics. The cells were cultured for 14 days at 37 °C with 5% CO₂ and the media was changed three times per week.

2.8. Cell viability

Cell viability by determination of lactate dehydrogenase (LDH) activity in cell culture medium was measured using the manufacturer's protocol (Pierce LDH Cytotoxicity Assay Kit, Thermo scientific, USA). After one and three days, 50 µl cell culture was collected. The absorbance was measured at 490 nm and the background at 680 nm was subtracted. Cytotoxicity is calculated as a percentage from total cell death. For each time point the maximum LDH activity was measured from cells cultured in well plates. Cells were lysed with specific buffer from the kit. Scaffolds without salt were used to measure the spontaneous LDH activity. The final %Cytotoxicity was calculated by

$$\% \text{Cytotoxicity} = \frac{[\text{Compound} - \text{treated LDH activity}] - [\text{Spontaneous LDH activity}]}{[\text{Maximum LDH activity}] - [\text{Spontaneous LDH activity}]} \cdot (100)$$

Live/dead cell staining was used to determine viability of the adherent cells. The cells were first washed with PBS and then stained using calcein AM (1:500) and propidium iodide (PI; 1:1000) diluted in PBS. After 30 min, protected from light and incubated at RT, samples were washed with PBS and observed using confocal microscopy.

2.9. Real-time PCR

After 14 days of cell culture, total RNA was isolated using Ribozol (Amresco, Solon, OH, USA), according to the manufacturer's protocol.

Table 1
Primer sequences used for real-time PCR analysis.

Gene	Primer sequence	
Glyceraldehyde-3-phosphate dehydrogenase (GAPDH)	hGAPDH-F	GGGAGCCAAAAGGTCATCA
	hGAPDH-R	GCATGGACTGTGGTCATGAGT
β -actin	hBActin-F	CTGGAACGGTGAAGGTGACA
	hBActin-R	AAGGGACTTCTGTAAACAA
Collagen I $\alpha 1$ (COL1)	hCOL1A1-F	CCCCAGCCACAAGAGTCTAC
	hCOL1A1-R	TTGGTGGGATGTCTTCGTCT
Alkaline phosphatase (ALP)	hALP-F	GAAGGAAAAGCCAAGCAGGC
	hALP-R	GGGGGCCAGACCAAGATAG
Runt related transcription factor 2 (RUNX2)	hRUNX2-F	TTCCAGACCAGCAGCACTC
	hRUNX2-R	CAGCGTCAACACCATCATTC

Total RNA was quantified at 260 nm using a nanodrop spectrophotometer (Thermo Scientific, Wilmington, DE, USA). The same amount of RNA (1 μ g) was reverse transcribed to cDNA according to the protocol of the supplier (qScript cDNA Synthesis Kit, Quanta Biosciences). Aliquots of diluted cDNA sample were used for the later real-time PCR (Realplex, Eppendorf, Germany) reactions for two reference genes and target genes (see Table 1). Each reaction contained 7 μ l of master mix (Perfecta SYBR Green FastMix, Quanta Biosciences), the sense and the antisense specific primers (20 μ M) and cDNA sample (3 μ l) in a final volume of 10 μ l. The amplification program consisted of a pre-incubation step for denaturation of the template cDNA (2 min 95 $^{\circ}$ C), followed by 40 cycles consisting of a denaturation step (5 s 95 $^{\circ}$ C), an annealing step (15 s 60 $^{\circ}$ C) and an extension step (20 s 72 $^{\circ}$ C). After each cycle, fluorescence was measured at 72 $^{\circ}$ C. A negative control without cDNA template was run in each assay.

All samples were normalized by the geometric mean of the expression levels of β -actin and GAPDH and fold changes were related to the control group using the following equation:

$$\text{ratio} = \frac{(E_{\text{target}})^{\Delta C P_{\text{target}}(\text{control-sample})}}{(E_{\text{ref}})^{\Delta C P_{\text{ref}}(\text{control-sample})}}$$

adapted from [9], where CP is the crossing point of the reaction amplification curve and E is the efficiency from the given slopes using serial dilutions. Stability of reference genes was calculated using a statistical tool (BestKeeper software, Technical University of Munich, Weihenstephan, Germany) [10].

2.10. Statistics

Compressive strength results are shown as mean \pm standard deviation. Statistical analysis was performed using one-way analysis of variance (ANOVA) and pairwise multiple comparison by using Holm-Sidak method. If the normality (Shapiro-Wilk) or equal variance

(Brown-Forsythe) test failed, Kruskal-Wallis one way analysis of variance on ranks was performed followed by pairwise comparison using Tukey Test. Cell results are shown as mean \pm standard deviation of the mean. Statistic was performed using paired *t*-test and normality test using Shapiro-Wilk.

3. Results and discussion

3.1. Grain boundary corrosion and its effect on compressive strength

We have previously shown that cationic doping leads to a significant increase in compressive strength and the formation of a distinct grain boundary phase rich in the dopant ions in porous TiO₂ bone scaffolds [5]. Other studies have shown, that an acidic environment, which may occur for example during the inflammatory phase of bone healing, causes corrosion confined to grain boundaries [11,12]. Ceramics corrode via ion leaching and dissolution, which leads to a release of impurity ions from the grain boundaries. Additionally, corrosion in grain boundaries results in a significant decrease in compressive strength [8]. Considering the new grain boundary formation with a high concentrations of impurity ions at grain boundaries, the corrosion behavior of cation doped TiO₂ scaffolds was investigated in this study.

Ca and Sr doped scaffolds did not show any corrosion or change in compressive strength when stored in dH₂O (Figs. 1 and 2). The compressive strength was stable over 8 weeks and grain boundaries did not show any dissolutions. However, when Ca and Sr scaffolds were stored in an acidic environment, grain boundary corrosion was present. These groups corroded via ion leaching and dissolution, which resulted in a significant decrease in compressive strength. No further change in grain boundary dissolution or compressive strength was observed after two weeks, when stored in the same solution. This shows that grain boundary corrosion occurred already within the first two weeks. Although the change in the compressive strength caused by the corrosion was similar for Ca and Sr doped scaffolds, the remaining grain boundaries, and therefore, the grain boundary morphology were different. While Ca doped scaffolds showed corrosion resistant lamellae in corroded grain boundaries, Sr doped scaffolds exhibited an uneven corrosion resistant layer. To explain both of these mechanisms occurring in the doped grain boundaries, TEM analysis was performed and the results are shown in Fig. 3. Ca doped scaffolds showed an amorphous phase rich in Ca, Al and Si. The observed Al and Si in the grain boundary phase are considered to originate from the sintering environment as previously discussed by Müller et al. [8]. Additionally, TiO₂ crystals were found in grain boundary regions with direct contact to grains, indicating that corrosion resistant TiO₂ lamellar structures were forming in the grain boundaries of the Ca doped scaffolds. The amorphous phase consisting of Ca, Si and Al in between these lamellae was dissolved when stored in acidic solution. This ion leaching and

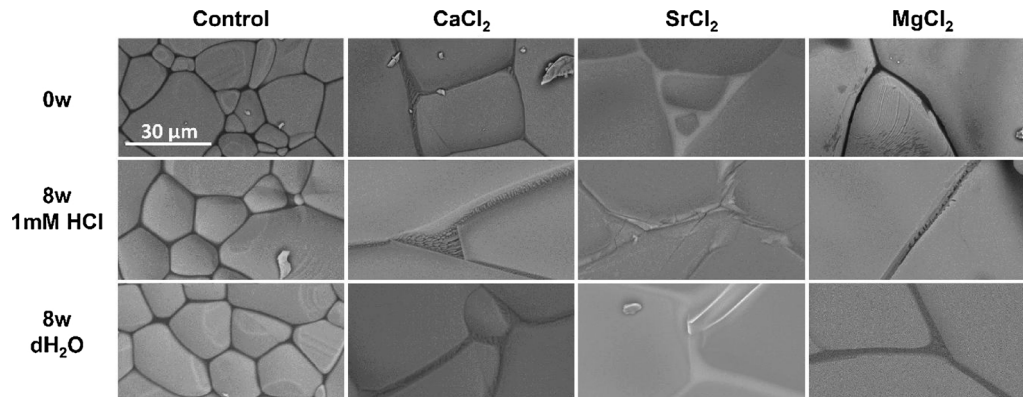


Fig. 1. Grain boundaries of uncorroded (0 w) and corroded (8 w-1 mM HCl and dH₂O) scaffolds as observed by SEM. Corrosion was concentrated in grain boundaries after storing in 1 mM HCl solution.

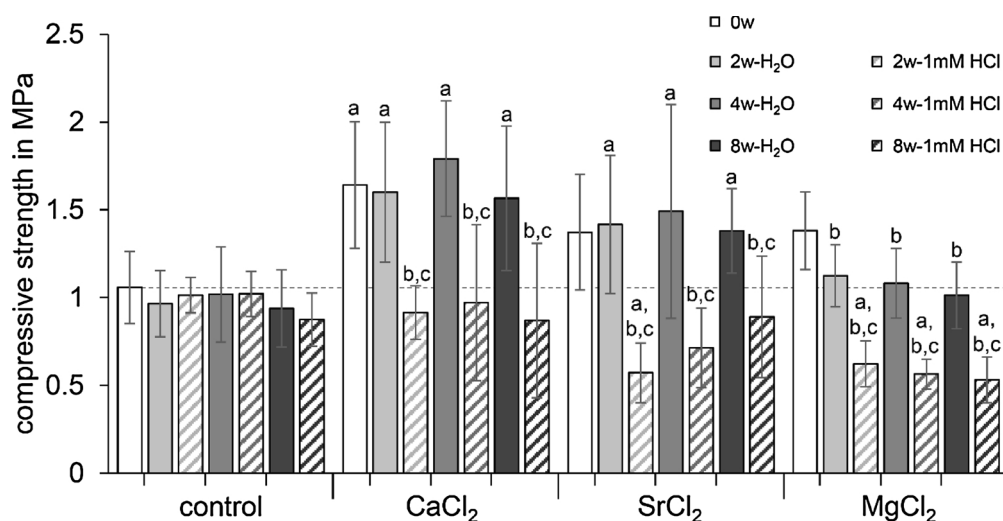


Fig. 2. Compressive strength of long-term treated (2, 4 and 8 weeks in dH₂O and 1 mM HCl) scaffolds doped with 0.1 M CaCl₂, SrCl₂ and MgCl₂. Significant difference ($p < 0.001$, $n = 10$) is indicated in comparison to control scaffolds with the same treatment and same time point (a), to uncorroded scaffolds with same doping (b) and to dH₂O groups at the same time point (c).

dissolution resulted in the decreased compressive strength. Formation of a new crystalline grain boundary phase was detected in the Sr doped scaffolds (Fig. 3C–E). SrTiO₃ crystals and an amorphous phase rich in Al and Si were observed in Sr doped grain boundaries. Considering the SEM images presented in Fig. 1, the ion leaching and dissolution was concentrated in the amorphous phase, causing the significant reduction in compressive strength, while the more corrosion resistant SrTiO₃ crystals remained intact after storage in acidic solution.

Mg doped TiO₂ scaffolds showed a different corrosion behavior compared to Ca and Sr doped scaffolds. As shown in Fig. 1, the corrosion was confined to the Mg rich spots within the grain boundary, resulting in small and localised holes in the grain boundary phase rather than the more homogeneous dissolution of an amorphous grain boundary phase seen in Ca and Sr doped scaffolds. The different observed

corrosion mechanism compared to the Ca and Sr doped scaffolds was found to influence the compressive strength in a different way as well. More importantly, a significant decrease in compressive strength already occurred after storing these scaffolds in dH₂O. This reduction in strength was even more pronounced following exposure to 1 mM HCl (Fig. 2).

The different corrosion behavior in Mg doped scaffolds was confirmed by measuring the released ions after the corrosion test (Fig. 4). While the amount of released Ca and Sr ions did not increase after three days, the amount of released Mg was significantly increased after three days. This indicates that Mg doped grain boundaries exhibit a new phase, which is more corrosion resistant compared to Ca and Sr doped grain boundary phases, resulting in a slower and more continuous release of Mg ions. A similar result was published by Gavrilov et al., who

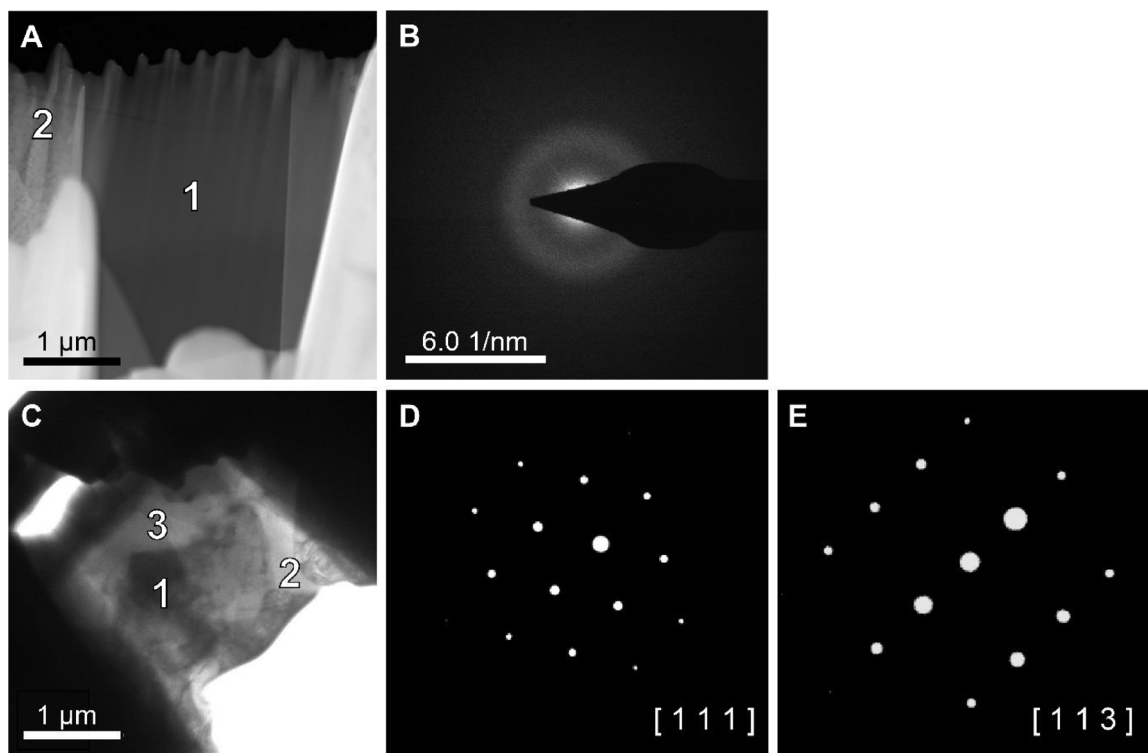


Fig. 3. TEM images of 0.1 M CaCl₂ and SrCl₂ scaffold grain boundary. CaCl₂ sample showed (A) showed an amorphous phase rich in Al, Si and Ca (1) and TiO₂ crystals (2). No diffraction was observed in the amorphous phase rich in Ca (B). The SrCl₂ sample (C) contains SrTiO₃ (1), TiO₂ (3) crystals and an amorphous part rich in Si and Al (2). The selected area diffraction (SAD) pattern confirmed the crystal structure of SrTiO₃ and shows the planes [111] (D) and [113] (E).

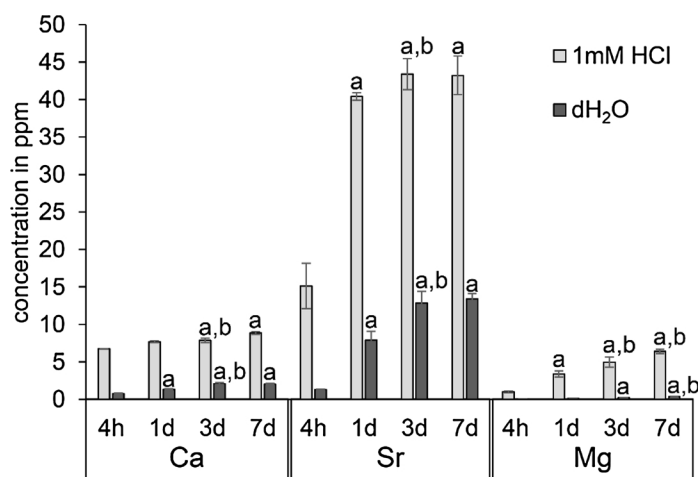


Fig. 4. Cumulative released ion profiles of doped TiO₂ scaffolds (n = 3) stored in 4 ml pH3 solution and dH₂O for different time points. Significant difference (p < 0.001, n = 6) is indicated in comparison to the earliest time point (4 h) (a) and to one time point earlier (b).

improved the corrosion resistance of alumina due to MgO doping [13]. Although the new grain boundary phase present in Mg doped scaffolds seemed to be more corrosion resistant compared to other doped scaffolds based on observed prolonged release of Mg, this phase did not result in a stable compressive strength of doped scaffolds stored in dH₂O or 1 mM HCl.

3.2. Effect of salt concentration on grain boundary development and corrosion behavior

In accordance to Müller et al. [8], our results showed that ion leaching and dissolution confined to grain boundaries resulted in the release of impurity ions from the grain boundaries. Furthermore, the present study showed that the dissolution of these impurity ions occurred whether a crystalline or amorphous phase was present at the grain boundary. To understand the development of these phases present in the grain boundaries, scaffolds with incrementally increasing salt concentration were tested. Additionally, the corrosion behavior was tested to correlate grain boundary phase development and corrosion in cation doped TiO₂ scaffolds.

The development of the grain boundary phase in all three doped scaffolds groups was similar. No changes in the grain boundaries were observed for 0.02 and 0.04 M scaffolds, which was consistent with the similar compressive strength of these scaffolds compared to undoped scaffolds (Figs. 5 and 6). By increasing the concentration to 0.06 M, the grain boundary formation changed and the distinct grain boundary formation started to form. Especially after exposing these scaffolds to 1 mM HCl, the new grain boundary formation and the characteristic dopant dependent corrosion resulted in a significant decreased compressive strength. The amorphous phase forming in Ca doped scaffolds was homogeneously distributed until the Ca ion concentration of 0.08 M. SEM images and the slightly decrease in the compressive strength after corrosion confirmed a homogeneous distribution and dissolution of the amorphous phase. With a concentration of 0.1 M, the previously described TiO₂ lamellae start to form and the resulting change from a homogeneous to a localised dissolution of the amorphous phase between these lamellae caused a significant decrease in compressive strength. The presence of a crystalline grain boundary phase in Sr doped scaffolds was increased with increased dopant concentration. The increasing amount of crystalline SrTiO₃ led to a more localised corrosion resulting in deep holes in the grain boundary, as previous described. Sr and Mg doped scaffolds showed a similar development at grain boundaries: the higher the salt concentration the higher the amount of the SrTiO₃ crystals or Mg rich spots. One explanation for this could be that the more corrosion resistant phase forming in Mg doped

scaffolds consisting of MgTiO₃ crystals. Because of the sintering parameters, such as holding temperature and cooling rate, the formation of MgTiO₃ crystals may not be sufficient to reach similar amount of crystalline MgTiO₃ compared to the SrTiO₃ in the Sr doped scaffolds.

Overall, corrosion was observed in all doped scaffolds in the form of ion leaching and dissolution. Because of a more corrosion resistant behavior of crystalline structures, the corrosion was concentrated in amorphous regions. Furthermore, with increasing impurity content in grain boundaries, the decrease in binding energy causes corrosion concentrated in these areas [14]. Fig. 7 summarizes the most important corrosion mechanism. Ca doped scaffolds showed a homogeneous removal of material in grain boundaries, while Sr and Mg doped scaffolds showed a concentrated and deep corrosion in the amorphous areas between the crystalline phases. Furthermore, the formation of the characteristic grain boundaries led to higher structural densification and significant higher compressive strength. Simultaneously, the significant loss in compressive strength caused by the corrosion was strongly correlated to the specific grain boundary formation. No optimal compromise between increased compressive strength and corrosion resistance could be observed.

3.3. Cell response in the presence of released ions

The prepared TiO₂ bone scaffolds doped with divalent cations feature high interconnected pore volume with porosity of approximately 90% and average pore size exceeding 420 μm [5]. Previous studies showed that such TiO₂ bone scaffolds are osteoconductive and show osteogenic potential. Osteoconductivity was confirmed *in vivo* due to direct contact of bone and scaffold material [2], while *in vitro* tests showed the support of TiO₂ scaffolds on osteogenic differentiation of MC3T3-E1 pre-osteoblasts without osteogenic supplements [15]. Furthermore, human mesenchymal stem cells (hMSCs) cultured on TiO₂ scaffolds showed significant higher cell viability and proliferation compared to hMSCs cultured on commercially available bone graft granules [16]. Considering these results with other studies showing a positive influence of TiO₂ scaffolds on osteosarcoma cells (SaOs-2) and normal human osteoblasts (NHO) differentiation [17,18], the analysis of this study was focused on the influence of released ions while undoped TiO₂ scaffolds were used as a control. The used ions were expected to have a positive influence on osteogenic differentiation, because of their important role in bone biology [19–21]. An increased osteogenic differentiation in the presence of ions like Ca, Sr and Mg has been shown in previous studies [22,23]. An increased extracellular calcium concentration can cause an increase of intracellular calcium through calcium channels and results in activation of important targets

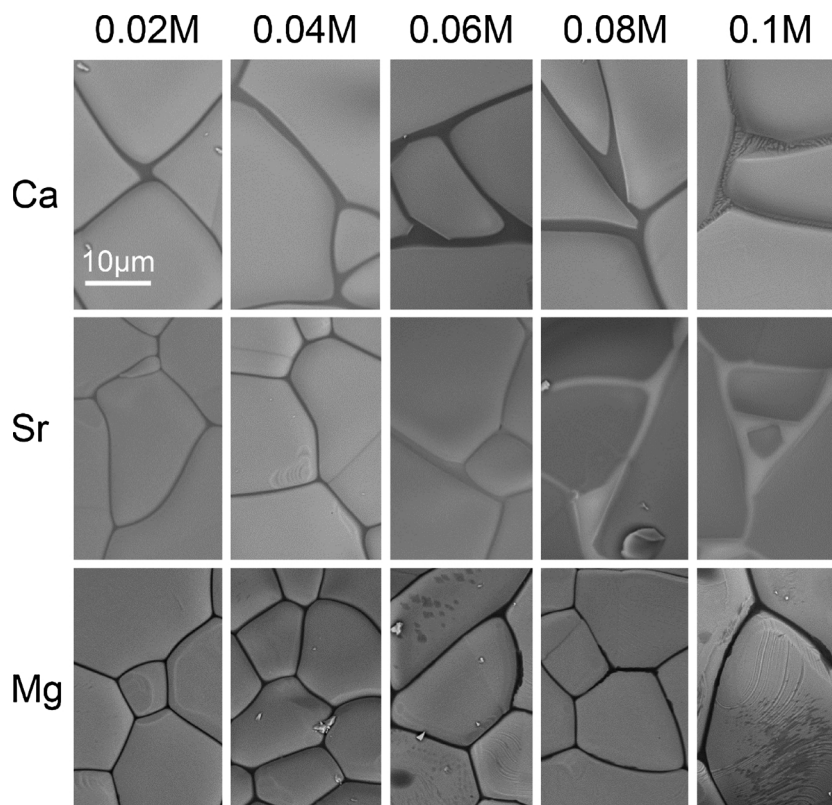


Fig. 5. Development of grain boundary morphology as observed by SEM depending on salt concentration in Ca, Sr and Mg doped TiO_2 scaffolds.

during osteogenic differentiation [24]. Strontium affects DNA synthesis and bone collagen synthesis strongly depending on the concentration [25]. Furthermore, strontium has a physical and chemical similarity to calcium and can increase osteoblast markers and matrix mineralization [26]. Besides the crucial role of magnesium in bone remodelling and skeletal development, the presence of increased magnesium concentration showed to increase osteoblast adhesion to implants [27,28].

In the present study, live dead staining and LDH activity, as a marker of cytotoxicity, showed no difference between the doped and undoped groups (Fig. 8). Next, the influence of released ions on hASCs osteogenic differentiation was studied. Gene expression analysis revealed that cells cultured on Mg doped scaffolds as a significant higher mRNA expression level of the osteogenic markers RUNX2, COL1 and ALP (Fig. 9).

The osteogenic differentiation requires the expression of the transcription factor RUNX2 to trigger the expression of later key osteogenic markers [29]. Among these, collagen type I, which is an essential component of the bone ECM, is produced. This is followed by an increased ALP expression which indicates the organization of the bone ECM and arrangement for mineralization. While RUNX2 and COL1 are early markers of osteogenic differentiation with a peak during proliferation, ALP is upregulated during extracellular matrix mineralization, maturation and organization [30]. Therefore, these genes are differently expressed during differentiation and can be used to determine the stage of osteoblast development. Thus, the real-time PCR results for the Mg group could be an indication for the differentiation of hASCs into the osteogenic lineage due to a significant higher gene expression level of the key osteogenic markers. A limitation of the present study is the measurement of one time point, what did not allow a time depending peak measurement of expressed genes. A peak in BSP expression would confirm fully differentiated osteoblasts [29]. The higher but not significant BSP expressions could lead to the assumption that the cells have not yet reached a fully differentiated state. In conclusion, Mg doping of TiO_2 scaffolds showed an increased osteogenic

differentiation in hASCs.

This effect was not observed for cells seeded on Sr or Ca doped scaffolds although they showed a higher amount of released ions. A possible explanation could be that hASCs are more sensitive to Mg ions and a lower amount influences the cells in a significant increase in specific gene expressions. Previous studies showed different cell responses to different ions and their concentrations in vitro. While Wang et al. showed an improved cell response correlated with increasing the magnesium ion concentration, Aimaiti et al. demonstrated that a low concentration of strontium stimulates the cells whereby a high concentration cause apoptosis [31,32]. Another reason could be the different release profile of doped scaffolds. Although the amount of Ca and Sr ions is higher, after 3 days no further release was observed. Because of the need of media change during cell studies, the released ions were removed after 3 days. On the other hand, Mg doped scaffolds showed a different release profile and a significant increase in released ions after 3 days. Therefore, Mg is the only group that differs from the control scaffolds from that time point on, suggesting that the released Mg ions can promote osteogenic differentiation of hASCs.

4. Conclusion

The corrosion in doped TiO_2 scaffolds confined to grain boundaries. Sr doping resulted in a new crystalline SrTiO_3 phase present in amorphous Si and Al rich grain boundaries. After exposure to an acidic solution, ion leaching and dissolution took place in the amorphous regions of the grain boundary phase. The removal of material in small areas led to deep holes and a significant decrease in compressive strength. The corrosion effect was similar for Mg doped scaffolds. Ca doping resulted in an amorphous phase rich in Ca, Al and Si. The corrosion in these purely amorphous grain boundaries was homogenous throughout the entire grain boundary region. Although the corrosion behavior was different, grain boundary corrosion resulted in a decreased compressive strength for all doped scaffolds. The effect of the

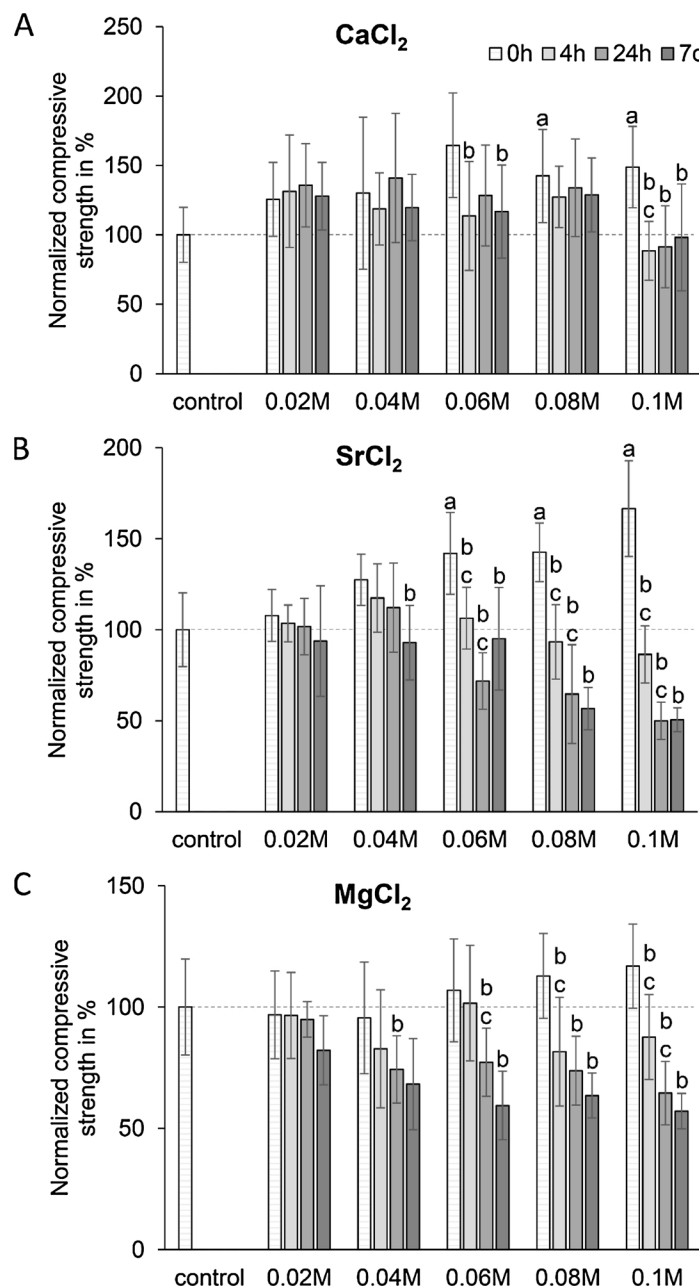


Fig. 6. Normalized compressive strength of Ca (A), Sr (B) and Mg (C) doped scaffolds with increasing doping concentration after short term corrosion test in 1 mM HCl. Significant differences ($p < 0.001$, $n = 10$) compared to the control scaffolds (a), to the same concentration at 0 h (b) and to the same concentration at one time point earlier (c) are highlighted.

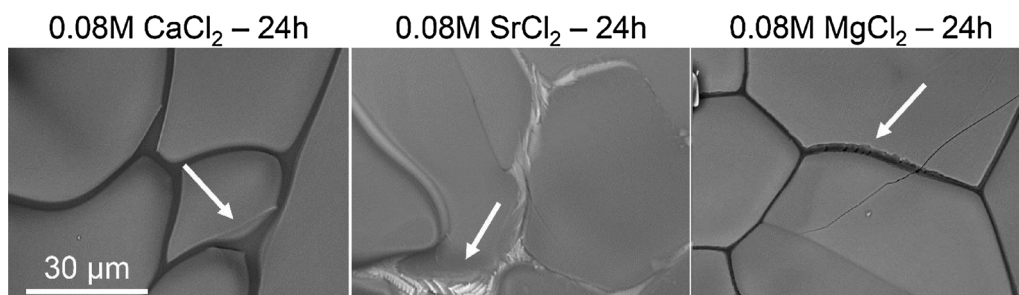


Fig. 7. Highlights of corroded scaffolds, doped with 0.08 M of different salts. CaCl₂ scaffolds showed homogeneous ‘washed out’ grain boundaries. SrCl₂ and MgCl₂ showed concentrated corrosion in amorphous parts of the grain boundary.

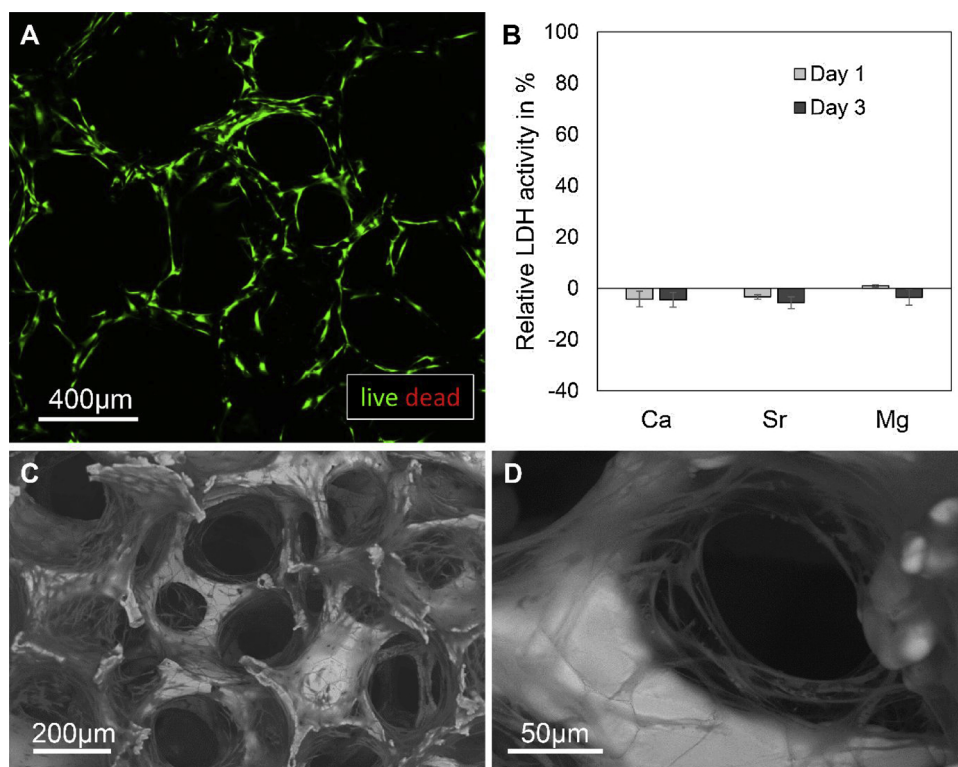


Fig. 8. Cell viability of hASCs cultured on cationic doped TiO₂ scaffolds. Live dead staining shows mainly living cells on control scaffolds after day 3 (A). The relative LDH activity in % showed that none of the doped groups showed any cytotoxic effect on hASCs (B). SEM images confirmed the growth of hASCs inside MgCl₂ scaffolds (C) and along the struts in CaCl₂ (D) after 14 days. No observed difference in tested groups, therefore, images A, C and D are representative for all tested groups.

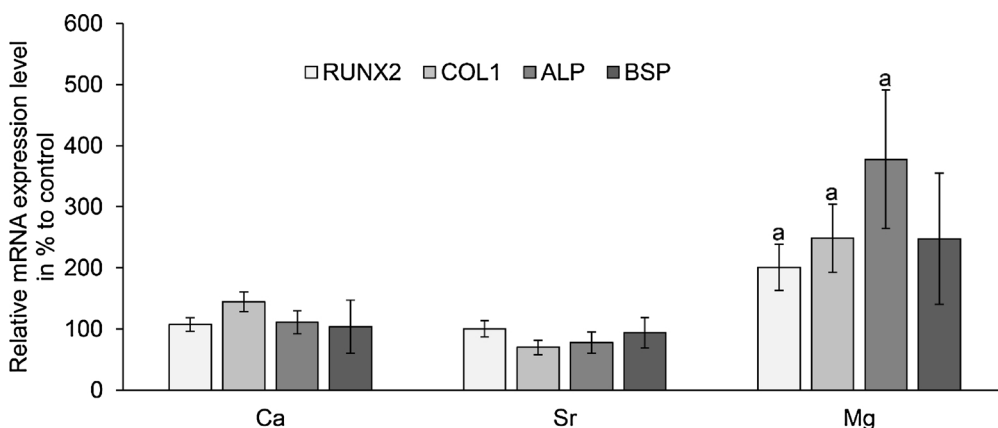


Fig. 9. Relative mRNA levels of RUNX2, COL1, ALP and BSP in hASCs cultured on doped TiO₂ scaffolds after 14 days. The expression level is given as % compared to cells cultured on undoped control scaffolds (100% expression). Cells seeded on Mg doped scaffolds showed a significant higher level in COL1, ALP and RUNX2 after 14 days compared to cells seeded on undoped scaffolds. a: $p < 0.05$, $n = 4$.

higher densification of TiO₂ in the presence of additional ions such as Ca, Sr and Mg and the resulting significant increase in compressive strength was found to be strongly depending on the new grain boundary formation. This new grain boundary formation caused a lower corrosion resistance and a significant decrease in compressive strength after corrosion. An optimal compromise between an increased compressive strength and corrosion resistant was not found.

The amount of released ions did not show any cytotoxic effect on hASCs. Released Mg ions showed a positive influence on hASCs, resulting in a significant increased osteogenic differentiation.

Acknowledgements

The authors thank Rui Domingues and Ana Gonçalves for their excellent technical assistance with confocal and real-time PCR. The authors acknowledge UiO:Life Science and Erasmus+ staff mobility for providing traveling grants for Anne Klemm to perform experiments at 3B's Research Group, Univeristy of Minho.

References

- [1] H. Haugen, J. Will, A. Köhler, U. Hopfner, J. Aigner, E. Wintermantel, Ceramic TiO₂-foams: characterisation of a potential scaffold, *J. Eur. Ceram. Soc.* 24 (4) (2004) 661–668.
- [2] H. Tiainen, J.C. Wohlfahrt, A. Verket, S.P. Lyngstadaas, H.J. Haugen, Bone formation in TiO₂ bone scaffolds in extraction sockets of minipigs, *Acta Biomater.* 8 (6) (2012) 2384–2391.
- [3] H.J. Haugen, M. Monjo, M. Rubert, A. Verket, S.P. Lyngstadaas, J.E. Ellingsen, H.J. Rønold, J.C. Wohlfahrt, Porous ceramic titanium dioxide scaffolds promote bone formation in rabbit peri-implant cortical defect model, *Acta Biomater.* 9 (2) (2013) 5390–5399.
- [4] H. Tiainen, D. Wiedmer, H.J. Haugen, Processing of highly porous TiO₂ bone scaffolds with improved compressive strength, *J. Eur. Ceram. Soc.* 33 (1) (2013) 15–24.
- [5] A. Klemm, H. Tiainen, Coagulated concentrated anatase slurry leads to improved strength of ceramic TiO₂ bone scaffolds, *Ceram. Int.* 44 (6) (2018) 6265–6271.
- [6] I. Silver, R. Murrills, D. Etherington, Microelectrode studies on the acid micro-environment beneath adherent macrophages and osteoclasts, *Exp. Cell Res.* 175 (2) (1988) 266–276.
- [7] W.B. White, Theory of Corrosion of Glass and Ceramics, *Corrosion of Glass, Ceramics and Ceramic Superconductors*, (1992), pp. 2–28.
- [8] B. Müller, H. Haugen, S.L. Simonsen, H. Tiainen, Grain boundary corrosion of highly porous ceramic TiO₂ foams is reduced by annealing and quenching, *J. Eur. Ceram. Soc.* 36 (1) (2016) 179–188.

- [9] M.W. Pfaffl, A new mathematical model for relative quantification in real-time RT-PCR, *Nucleic Acids Res.* 29 (9) (2001) e45–e45.
- [10] M.W. Pfaffl, A. Tichopad, C. Prgomet, T.P. Neuvians, Determination of stable housekeeping genes, differentially regulated target genes and sample integrity: BestKeeper–excel-based tool using pair-wise correlations, *Biotechnol. Lett.* 26 (6) (2004) 509–515.
- [11] L. Čurković, M.F. Jelača, S. Kurajica, Corrosion behavior of alumina ceramics in aqueous HCl and H₂SO₄ solutions, *Corros. Sci.* 50 (3) (2008) 872–878.
- [12] K.R. Mikeska, S.J. Bennison, S.L. Grise, Corrosion of ceramics in aqueous hydrofluoric acid, *J. Am. Ceram. Soc.* 83 (5) (2000) 1160–1164.
- [13] K.L. Gavrilov, S.J. Bennison, K.R. Mikeska, J.M. Chabala, R. Levi-Setti, Silica and magnesia dopant distributions in alumina by high-resolution scanning secondary ion mass spectrometry, *J. Am. Ceram. Soc.* 82 (4) (1999) 1001–1008.
- [14] Y. Takigawa, Y. Ikuhara, T. Sakuma, Grain boundary bonding state and fracture energy in small amount of oxide-doped fine-grained Al₂O₃, *J. Mater. Sci.* 34 (9) (1999) 1991–1997.
- [15] M. Gómez-Florit, M. Rubert, J.M. Ramis, H.J. Haugen, H. Tiainen, S.P. Lyngstadaas, M. Monjo, TiO₂ scaffolds sustain differentiation of MC3T3-E1 cells, *J. Biomater. Tissue Eng.* 2 (4) (2012) 336–344.
- [16] R. Sabetrasekh, H. Tiainen, S.P. Lyngstadaas, J. Reseland, H. Haugen, A novel ultra-porous titanium dioxide ceramic with excellent biocompatibility, *J. Biomater. Appl.* 25 (6) (2011) 559–580.
- [17] B. Müller, J.E. Reseland, H.J. Haugen, H. Tiainen, Cell growth on pore-graded biomimetic TiO₂ bone scaffolds, *J. Biomater. Appl.* 29 (9) (2015) 1284–1295.
- [18] A. Verket, H. Tiainen, H.J. Haugen, S.P. Lyngstadaas, O. Nilsen, J.E. Reseland, Enhanced osteoblast differentiation on scaffolds coated with TiO₂ compared to SiO₂ and CaP coatings, *Biointerphases* 7 (1–4) (2012) 36.
- [19] S.P. Nielsen, The biological role of strontium, *Bone* 35 (3) (2004) 583–588.
- [20] H.C. Blair, L.J. Robinson, C.L.H. Huang, L. Sun, P.A. Friedman, P.H. Schlesinger, M. Zaidi, Calcium and bone disease, *Biofactors* 37 (3) (2011) 159–167.
- [21] S. Castiglioni, A. Cazzaniga, W. Albisetti, J.A. Maier, Magnesium and osteoporosis: current state of knowledge and future research directions, *Nutrients* 5 (8) (2013) 3022–3033.
- [22] A.J. Leite, A.I. Gonçalves, M.T. Rodrigues, M.E. Gomes, J.F. Mano, Strontium doped bioactive glass nanoparticles in osteogenic commitment, *ACS Appl. Mater. Interfaces* (2018).
- [23] H. Gu, F. Guo, X. Zhou, L. Gong, Y. Zhang, W. Zhai, L. Chen, L. Cen, S. Yin, J. Chang, The stimulation of osteogenic differentiation of human adipose-derived stem cells by ionic products from akermanite dissolution via activation of the ERK pathway, *Biomaterials* 32 (29) (2011) 7023–7033.
- [24] G.-Y. Jung, Y.-J. Park, J.-S. Han, Effects of HA released calcium ion on osteoblast differentiation, *J. Mater. Sci.: Mater. Med.* 21 (5) (2010) 1649–1654.
- [25] P. Marie, P. Ammann, G. Boivin, C. Rey, Mechanisms of action and therapeutic potential of strontium in bone, *Calcif. Tissue Int.* 69 (3) (2001) 121–129.
- [26] P. Marie, D. Felsenberg, M. Brandi, How strontium ranelate, via opposite effects on bone resorption and formation, prevents osteoporosis, *Osteoporos. Int.* 22 (6) (2011) 1659–1667.
- [27] H. Zreiqat, C. Howlett, A. Zannettino, P. Evans, G. Schulze-Tanzil, C. Knabe, M. Shakibaei, Mechanisms of magnesium-stimulated adhesion of osteoblastic cells to commonly used orthopaedic implants, *J. Biomed. Mater. Res.* 62 (2) (2002) 175–184.
- [28] Y. Yamasaki, Y. Yoshida, M. Okazaki, A. Shimazu, T. Uchida, T. Kubo, Y. Akagawa, Y. Hamada, J. Takahashi, N. Matsuura, Synthesis of functionally graded MgCO₃ apatite accelerating osteoblast adhesion, *J. Biomed. Mater. Res.* 62 (1) (2002) 99–105.
- [29] R. Miron, Y. Zhang, Osteoinduction: a review of old concepts with new standards, *J. Dent. Res.* 91 (8) (2012) 736–744.
- [30] G.S. Stein, J.B. Lian, J.L. Stein, A.J. Van Wijnen, M. Montecino, Transcriptional control of osteoblast growth and differentiation, *Physiol. Rev.* 76 (2) (1996) 593–629.
- [31] G. Wang, J. Li, W. Zhang, L. Xu, H. Pan, J. Wen, Q. Wu, W. She, T. Jiao, X. Liu, Magnesium ion implantation on a micro/nanostructured titanium surface promotes its bioactivity and osteogenic differentiation function, *Int. J. Nanomedicine* 9 (2014) 2387.
- [32] A. Aimaiti, A. Maimaitiyiming, X. Boyong, K. Aji, C. Li, L. Cui, Low-dose strontium stimulates osteogenesis but high-dose doses cause apoptosis in human adipose-derived stem cells via regulation of the ERK1/2 signaling pathway, *Stem Cell Res. Ther.* 8 (1) (2017) 282.